Journal of Magnetism and Magnetic Materials 458 (2018) 164–170

Contents lists available at ScienceDirect

Journal of Magnetism and Magnetic Materials

journal homepage: www.elsevier.com/locate/jmmm

Research articles

Hydrothermal synthesis and magnetic properties of multiferroic $RMn_{0.5}Fe_{0.5}O_3$ (R = Tb, Dy, and Ho)

Li Guo, Zhiqiang Zhou *

College of Science, Northeast Forestry University, Harbin 150040, PR China

ARTICLE INFO

Article history:
Received 1 February 2018
Received in revised form 9 March 2018
Accepted 10 March 2018
Available online 12 March 2018

Keywords:
Multiferroic
Manganite
Spin reorientation
Magnetization reversal

ABSTRACT

Pure-phased orthorhombic $RMn_{0.5}Fe_{0.5}O_3$ (R = Tb, Dy, and Ho) were successfully synthesized via the low-temperature hydrothermal technique. The nucleation and crystal growth of $RMn_{0.5}Fe_{0.5}O_3$ (R = Tb, Dy, and Ho) were influenced mainly by medium alkalinity, reaction temperature and time. All the three samples are of orthorhombic structure with +3 valences of Mn and Fe. They present morphologies of spheres that are assembled by smaller tabular crystals. Spin reorientation transitions were observed in $RMn_{0.5}Fe_{0.5}O_3$ (R = Tb, Dy, and Ho), and magnetization reversal was observed in $TbFe_{0.5}Mn_{0.5}O_3$. The spin reorientation temperatures show a linear relation with the magnetic field intensity, and the spin reorientation and magnetization reversal disappear when the applied field is big enough. Antiferromagnetic transition of R^{3+} was observed in $TbFe_{0.5}Mn_{0.5}O_3$ and $DyFe_{0.5}Mn_{0.5}O_3$ at lower temperatures. All the three samples show the characteristics of spiral magnetic ordering at 2 K and show residual magnetism at both 2 K and 300 K.

© 2018 Elsevier B.V. All rights reserved.

1. Introduction

In recent years, people have done a lot of work in the synthesis and research of single-phased multiferroic materials that may integrate fine magnetism and ferroelectricity, and therein, some orthorhombic composite oxides such as rare-earth manganites ($RMnO_3$) [1–4], ferrites ($RFeO_3$) [5–12], etc. have become the research focus. Traditionally, ferroelectricity is considered to be forbidden in these centrosymmetric orthorhombic oxides. But ferroelectricity induced by special spontaneous polarization mechanisms has been discovered in some of these oxides, for example, ferroelectricity induced by spiral magnetic ordering in orthorhombic $DyMnO_3$ [13–19], induced by exchange contraction of Dy and Fe moments in orthorhombic $DyFeO_3$ has been reported [6,20–22].

In the orthorhombic, i.e. perovskite, structure, B-site ions of different electron configurations may provide diverse compositions and interactions, and therein, Fe and Mn are typical B-site magnetic elements. Fe^{3+} and Mn^{3+} have the same charge number and similar ionic radius, making Fe^{3+}/Mn^{3+} co-doping in BO_6 octahedra possible. A variety of exchange interactions such as Fe^{3+}–Fe^{3+}, Mn^{3+}–Mn^{3+}, Fe^{3+}–Mn^{3+}, R^{3+}–Fe^{3+}, R^{3+}–Mn^{3+}, R^{3+}–R^{3+} may exist in the B-site Fe^{3+}/Mn^{3+} co-doped rare-earth composite oxide $RMn_{1-x}Fe_xO_3$, and so more magnetic phase transitions may be expected, which is worthy of research. As we know, multiferroic occurs generally accompanied by magnetic phase transition [23–26]. The research of magnetic phase transitions may give us theoretical and experimental guidance in the search for multiferroic materials.

Orthorhombic $TbMnO_3$ [2], $DyMnO_3$ [3] and $HoMnO_3$ [4] are typical multiferroic candidates. In this work, orthorhombic $RMn_{0.5}Fe_{0.5}O_3$ (R = Tb, Dy, and Ho) were prepared via the hydrothermal technique, and the magnetic phase transitions were analyzed, which will provide some fundamental data for further research in this field.

2. Experimental

The starting materials were $Fe(NO_3)_3{\cdot}9H_2O$, $R(NO_3)_3{\cdot}6H_2O$ (R = Tb, Dy and Ho), $KMnO_4$, $MnCl_2$, and KOH. They were all analytically pure. For ensuring intensive mixing of the starting materials, the salts were used in the form of aqueous solutions. KOH was used as a mineralizer in its initial form of pellets. Here, we take $TbMn_{0.5}Fe_{0.5}O_3$ for example to demonstrate the synthesis route. $Fe(NO_3)_3$, $Tb(NO_3)_3$, and $KMnO_4$ solutions were mixed at room temperature, whose dosages were 10.00 mL, 5.00 mL and 3.33 mL, respectively, and whose concentrations were 0.40 M, 0.40 M and 0.12 M, respectively. KOH pellets were then gradually added into the mixture under strong stirring to reach a concentration of 20 M (molar number of KOH/initial solution volume). When

* Corresponding author.
E-mail address: zhouzq_nefu@163.com (Z. Zhou).

https://doi.org/10.1016/j.jmmm.2018.03.019
0304-8853/© 2018 Elsevier B.V. All rights reserved.

the above mixture reached room temperature, 2.86 mL $MnCl_2$ (0.56 M) was quickly added into it under stirring. The as-prepared mixture was transferred into a Teflon-lined stainless steel autoclave, and the filling degree was 80%. The autoclave was kept at 240 °C for 48 h to complete crystal nucleation and growth under autogenous pressure. And then, the autoclave was naturally cooled to room temperature. Ultrasonic separation and filtration were used to collect solid compounds from the autoclave. The solid compounds were thoroughly washed with deionized water to remove the soluble matters, and then dried in air at 60 °C to present the final samples. The synthesis routes of other samples were similar to that of $TbMn_{0.5}Fe_{0.5}O_3$.

A X-ray diffractometer (Rigaku D/Max 2500 V/PC) was employed to do powder X-ray diffraction (XRD), and the operation parameters were as follows: room temperature, 50 kV, 200 mA, Cu-K_α radiation ($\lambda = 1.5418$ Å), step scanning, increments of 0.02°, and angle range $20° \leq 2\theta \leq 80°$. A scanning electron microscope (SEM, JEOL JSM-6700F) operated at 5 kV was employed to observe the morphologies. Energy dispersive spectroscopy (EDS, attached to the above-said scanning electron microscope) was used to analyze the chemical compositions of the samples. X-ray photoelectron spectroscopy (XPS, Kratos AXIS Ultra DLD spectrometer) was used to analyze the element valences. Quantum Design MPMS-XL (SQUID) was used to record the zero-field-cooled (ZFC) and field-cooled (FC) curves with different density of sampling point.

3. Results and discussion

Many factors may influence the nucleation and crystal growth of $RMn_{0.5}Fe_{0.5}O_3$ (R = Tb, Dy and Ho), and the most dominant ones are medium alkalinity, reaction temperature and time. Higher alkalinity and higher temperature benefit the formation of $RMn_{0.5}Fe_{0.5}O_3$ (R = Tb, Dy, and Ho) while the reaction time produce no significant impact provided it is no less than 48 h. The reaction temperature and time should be no lower than 240 °C and no shorter than 48 h, or else, the main products shall be $R(OH)_3$, Fe_2O_3 and $K_xMnO_2{\cdot}yH_2O$.

The XRD patterns of the as-prepared samples are shown in Fig. 1. High degree of crystallization is indicated by the strong intensities and sharp shapes of the XRD patterns. From the embedded figure, we can see that the diffraction peaks shift to the high angle direction along with the decrease of R^{3+} radius. Indexation of the XRD data shows that all the three samples are of orthorhombic structure with space group Pnma. The lattice parameters were got through Pawley refinement, as shown in Table 1. Fig. 2 gives the Pawley refinement patterns of $HoMn_{0.5}Fe_{0.5}O_3$ as an example. The compositions of the samples were analyzed via EDS, as shown in Fig. S1 and Table S1. It can be seen that the molar ratios of R:Mn:Fe in the samples accord with the designed ratios in the starting materials.

XPS was used to analyze the valence states of Mn and Fe in the samples. Fig. 3 gives the Mn2p and Fe2p patterns of $DyMn_{0.5}Fe_{0.5}O_3$. The binding energy was corrected with standard C_{1s} (284.6 eV in room temperature). In Fig. 3(b), we can find two peaks at 710.8 eV and 724.3 eV which are ascribed to $Fe2p^{3/2}$ and $Fe2p^{1/2}$ from split of Fe2p. With reference to the standard database, these two peaks are consistent with that of Fe_2O_3, therefore, the valence of Fe was determined to be +3. Similarly, the valence of Mn was also determined to be +3. $TbMn_{0.5}Fe_{0.5}O_3$, $DyMn_{0.5}Fe_{0.5}O_3$ and $HoMn_{0.5}Fe_{0.5}O_3$ were prepared under the same conditions, and so we have the reason to believe that Mn and Fe in all the three samples show valence of +3 [27].

The SEM images of $RMn_{0.5}Fe_{0.5}O_3$ (R = Tb, Dy, and Ho) are given in Fig. 4. $TbMn_{0.5}Fe_{0.5}O_3$ and $DyMn_{0.5}Fe_{0.5}O_3$ take on morphologies

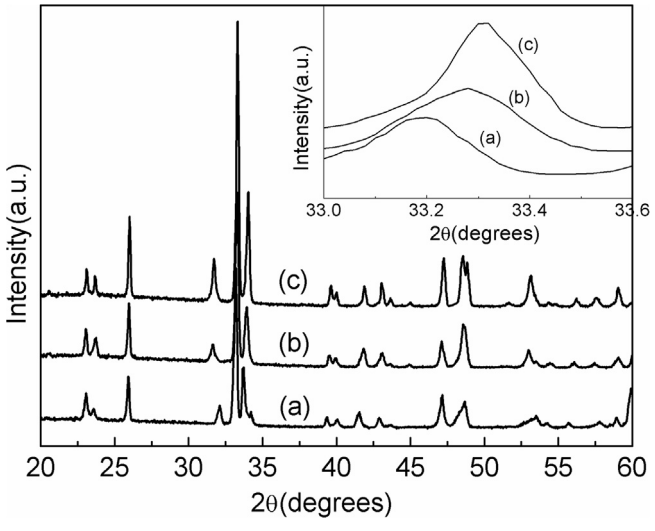

Fig. 1. The XRD patterns of $TbMn_{0.5}Fe_{0.5}O_3$ (a), $DyMn_{0.5}Fe_{0.5}O_3$ (b) and $HoMn_{0.5}Fe_{0.5}O_3$ (c); the insert is the magnified main peaks.

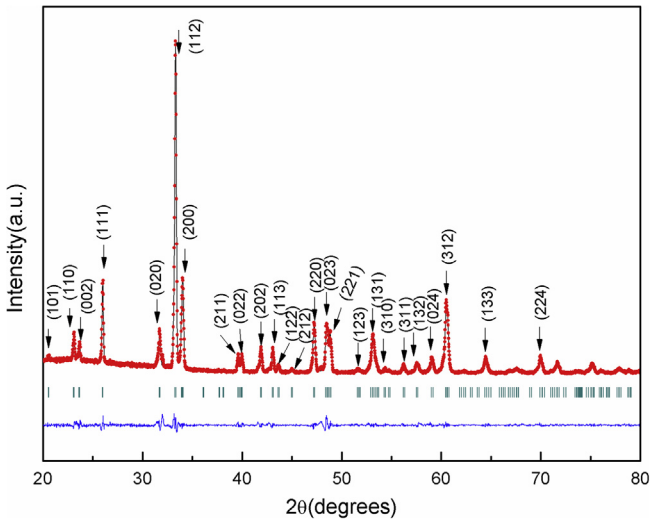

Fig. 2. Pawley Refinement Patterns of $HoMn_{0.5}Fe_{0.5}O_3$.

Table 1
Lattice parameters obtained from the powder XRD data.

	a	*b*	*c*	*V*	⟨*a*⟩	*D*
$TbMn_{0.5}Fe_{0.5}O_3$	5.5919(1)	7.5897(3)	5.3161(4)	225.63	5.4236	0.02044
$DyMn_{0.5}Fe_{0.5}O_3$	5.6155(1)	7.5396(3)	5.2979(2)	224.31	5.4130	0.024596
$HoMn_{0.5}Fe_{0.5}O_3$	5.6005(1)	7.5727(5)	5.2756(1)	223.75	5.4058	0.023182

Note: *a*, *b*, *c* are unite cell parameters; *D* denotes the orthorhombic distortion, $D = (1/3)\sum_i |a_i - \langle a\rangle|/\langle a\rangle$, a_i denoting *a*, *c* and $b/\sqrt{2}$, $\langle a\rangle = (abc/\sqrt{2})^{(1/3)}$.

Download English Version:

https://daneshyari.com/en/article/8153199

Download Persian Version:

https://daneshyari.com/article/8153199

Daneshyari.com